Time-dependent land uplift and subsidence in the Santa Clara valley, California, from a large interferometric synthetic aperture radar data set

David A. Schmidt[1] and Roland Bürgmann

Department of Earth and Planetary Science, University of California, Berkeley, California, USA

Received 28 October 2002; revised 20 March 2003; accepted 12 May 2003; published 5 September 2003.

[1] We invert 115 differential interferograms derived from 47 synthetic aperture radar (SAR) scenes for a time-dependent deformation signal in the Santa Clara valley, California. The time-dependent deformation is calculated by performing a linear inversion that solves for the incremental range change between SAR scene acquisitions. A nonlinear range change signal is extracted from the ERS InSAR data without imposing a model of the expected deformation. In the Santa Clara valley, cumulative land uplift is observed during the period from 1992 to 2000 with a maximum uplift of 41 ± 18 mm centered north of Sunnyvale. Uplift is also observed east of San Jose. Seasonal uplift and subsidence dominate west of the Silver Creek fault near San Jose with a maximum peak-to-trough amplitude of ~35 mm. The pattern of seasonal versus long-term uplift provides constraints on the spatial and temporal characteristics of water-bearing units within the aquifer. The Silver Creek fault partitions the uplift behavior of the basin, suggesting that it acts as a hydrologic barrier to groundwater flow. While no tectonic creep is observed along the fault, the development of a low-permeability barrier that bisects the alluvium suggests that the fault has been active since the deposition of Quaternary units. *INDEX TERMS:* 6924 Radio Science: Interferometry; 1829 Hydrology: Groundwater hydrology; 1884 Hydrology: Water supply; 5114 Physical Properties of Rocks: Permeability and porosity; 1243 Geodesy and Gravity: Space geodetic surveys; *KEYWORDS:* Santa Clara Valley, InSAR, time series, land subsidence

Citation: Schmidt, D. A., and R. Bürgmann, Time-dependent land uplift and subsidence in the Santa Clara valley, California, from a large interferometric synthetic aperture radar data set, *J. Geophys. Res.*, *108*(B9), 2416, doi:10.1029/2002JB002267, 2003.

1. Introduction

[2] The Santa Clara valley aquifer, located in the San Francisco Bay Area, represents a complex network of permeable, water-bearing units where groundwater is exchanged between units under different confining pressure (Figure 1). Fine-grained sediments deposited during periods of high sea level are interfingered with coarse-grained sediments derived from the surrounding uplands [*Clark*, 1924; *Iwamura*, 1995]. The layers of fine-grained interbeds consisting of mostly clay and silt restrict the vertical flow of groundwater. While groundwater flows more freely through the horizontal layers of sand and gravel, changes in stream channels during deposition disrupt the connectivity of the permeable units. The withdrawal or recharge of groundwater places the aquifer in a state of disequilibrium where hydraulic gradients drive flow. The time required to achieve equilibrium following a perturbation depends on the thickness, connectivity, and hydraulic diffusivity of permeable units [*Alley et al.*, 2002].

[3] The redistribution of groundwater produces a poroelastic response which can be observed as a surface deformation signal [*Rice and Cleary*, 1976]. Pore pressure changes, which are reflected by a change in head level, correspond to a change in the effective stress of the opposite sign. Therefore an increase in pore fluid pressure results in a decrease of the effective stress on the granular skeleton which supports the vertical load. As head levels increase or decrease, an elastic response is observed as either rebound or subsidence, respectively, of the surface typically on the order of cm.

[4] Inelastic deformation can also be observed in regions where excess groundwater pumping results in the compaction of previously saturated sediments. The pumping of groundwater from the aquifer reduces the pore pressure in the water-bearing units and the imposed hydraulic gradient drives groundwater out of the interbeds. The increase in the vertical effective stress within the interbed results in the irreversible compaction of compressible clay and silt units through the settling of grains [*Poland and Davis*, 1969]. The compaction can be observed as land subsidence with deformation on the order of meters for major aquifers.

[1]Now at Department of Geological Sciences, University of Oregon, Eugene, Oregon, USA.

0148-0227/03/2002JB002267$09.00

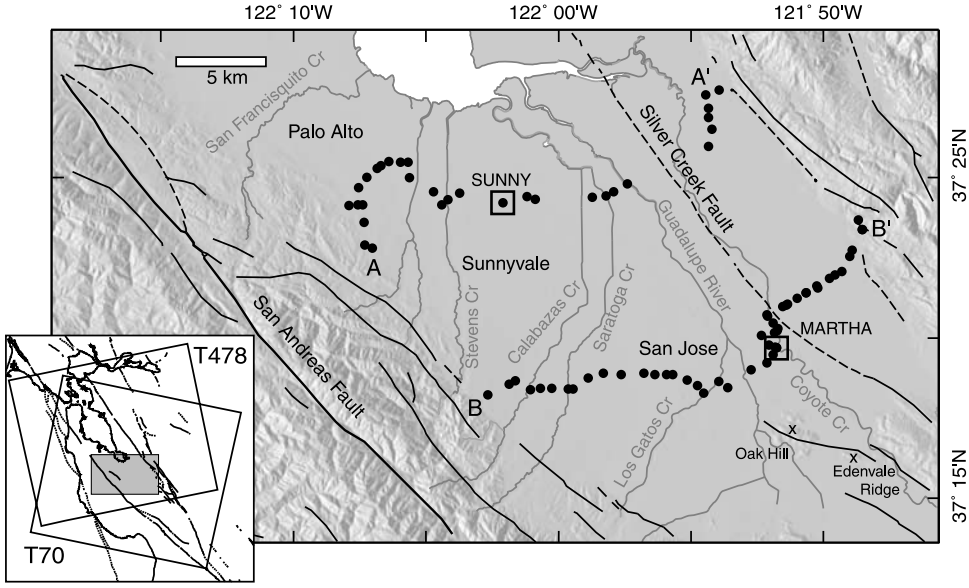

Figure 1. Shaded relief map of the Santa Clara valley. Bench mark locations are shown for two leveling lines (dots) and extensometer sites (open squares). All InSAR observations are referenced to Oak Hill. Faults appear as bold lines, dashed where inferred [*Jennings*, 1994]. Major drainage channels appear as gray lines. The inset shows the location of the Santa Clara valley (gray box) within the San Francisco Bay Area. The tilted rectangles identify the SAR frames along tracks 70 and 478.

[5] Interferometric synthetic aperture radar (InSAR) is an attractive method for observing deformation attributed to groundwater movements and land subsidence because it provides both a spatially and temporally rich data set [*Massonnet et al.*, 1997; *Fielding et al.*, 1998; *Galloway et al.*, 1998; *Amelung et al.*, 1999; *Bawden et al.*, 2001; *Hoffmann et al.*, 2001]. Under optimal conditions, a differential interferogram derived from two SAR scenes provides a spatially continuous measurement of the change in range between the satellite and the ground during a given time period [*Gabriel et al.*, 1989; *Massonnet et al.*, 1993]. These observational data provide a spatial sampling on the order of tens of meters, whereas level lines or GPS bench marks are typically more sparsely distributed. Since existing satellite systems repeat their orbit on the order of weeks, InSAR has the potential to resolve time-dependent deformation. However many InSAR studies have not utilized all of the available SAR data either because of the excess time required to process the interferograms or because of the lack of data analysis tools used to synthesize the information constrained in extensive InSAR data sets. New techniques that address the difficulties of dealing with large numbers of interferograms and extract a time-dependent signal are continuing to be developed by the community [*Beauducel et al.*, 2000; *Ferretti et al.*, 2000; *Lanari et al.*, 2002].

[6] In this paper, InSAR is used to resolve both the spatial and temporal pattern of uplift of the Santa Clara Valley aquifer over an 8-year period. We present a linear inversion scheme that solves for a range change time series using 115 differential interferograms. The abundance of InSAR data allows us to resolve both a seasonal and long-term pattern of uplift. The InSAR time series provides some insight on the mobility of groundwater within the aquifer and the distribution of permeable units.

2. Groundwater History of the Santa Clara Valley

[7] The Santa Clara Valley, located in the San Francisco Bay Area, has experienced a long history of land subsidence resulting from the excess pumping of groundwater [*Poland and Ireland*, 1988]. Beginning in the early 1900s, agriculture depended heavily on groundwater for irrigation. As farms were replaced by urban and industrial development in the 1940s, the extraction rate of groundwater continued to increase with the population. A decrease in rainfall during the first half of the twentieth century coupled with an increase in the rate of pumpage resulted in a substantial drop in artesian head levels by as much as 64 m from 1912 to 1966. This drop in head level was accompanied by as much as 4 m of land subsidence (Figure 2).

[8] The unchecked withdrawal of groundwater presented several social and economic problems. As the head levels dropped below sea level, the hydraulic gradient reversed direction away from San Francisco bay which raised concerns over saltwater intrusion. The compaction of fine-grained sediments in the aquifer caused well casings to fail under vertical compression. The subsidence redirected the flow of surface water requiring the redesign of flood control levees. The direct cost of these and other contingencies was estimated by *Fowler* [1981] to exceed $100 million.

[9] Recovery efforts since the 1960s have allowed water levels to partially recover while also stopping the compaction of sediments. The importation of outside sources of water through the construction of various state and municipal aqueducts provided a means to offset the effects of

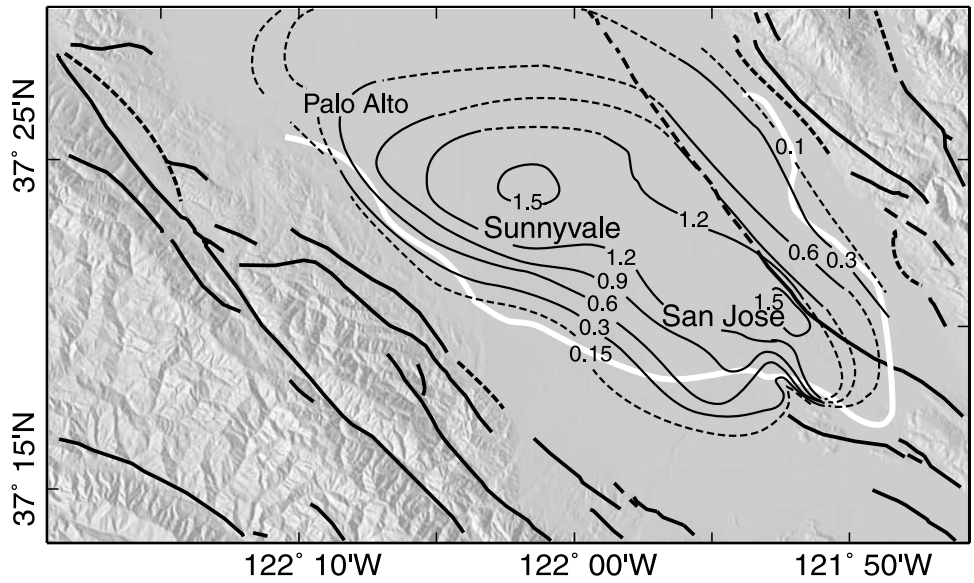

Figure 2. Land subsidence observed from 1934 to 1960 reproduced from *Poland and Ireland* [1988, Figure 19] using data collected by the National Geodetic Survey. Subsidence contours (thin lines, irregular intervals) are in units of m, dashed where poorly controlled. Regional faults and major cities are shown as in Figure 1. The spatial extent of the confined aquifer is denoted by the white line.

groundwater withdrawal. Percolation ponds were constructed on the margins of the valley to increase the recharge from winter runoff. A decrease in the rate of withdrawal and favorable rainfall totals also contributed to the recovery. By 1980, head levels had recovered by as much as 24 m. However, no significant uplift was observed as the head levels recovered illustrating the unrecoverable compaction of the interbeds. Prudent water management seeks to find the proper balance between groundwater withdrawal and recharge such that the compaction of sediments is minimized. InSAR data can provide observational evidence that compaction has ceased while also providing new insight into the dynamics of the groundwater system.

3. InSAR Methodology

[10] To observe the time-dependent deformation in the Santa Clara valley we processed 115 differential interferograms, which are distributed from June 1992 to September 2000 (Figure 3). Synthetic aperture radar (SAR) data were collected over the San Francisco Bay Area by the European Space Agency (ESA) using the ERS-1 and ERS-2 spacecraft. We chose to limit the number of interferograms used in the analysis to those with small perpendicular baselines (<200 m) to ensure that errors imposed by topography remain small. Interferograms are produced using the Repeat Orbit Interferometry Package (ROI PAC) developed at the Jet Propulsion Laboratory and the California Institute of Technology (JPL/Caltech). SAR data are processed using 8 looks in range and 40 looks in azimuth resulting in a pixel width of roughly 150 m. A weighted power spectral density filter and an adaptive filter are applied to each interferogram [*Goldstein and Werner*, 1998]. Processing parameters were chosen to counter temporal decorrelation in those interferograms spanning several years while maximizing resolution.

[11] Topography is removed from each interferogram using a 30 m U.S. Geological Survey (USGS) digital elevation model (DEM) and an evaluation of the elevation model suggests that imposed errors are negligible. A DEM of the Bay Area derived from the Shuttle Radar Topography Mapping (SRTM) mission was not available at the time that the interferograms were processed. Upon the recent release of the SRTM data a comparison was performed with the USGS DEM. A 50-km-wavelength signal with a maximum peak-to-trough amplitude of 2.7 m was found in the residual between elevation models for the flat, urban regions of the bay area. However, the analysis of tandem ERS InSAR data (1-day interferograms) suggests that this anomalous signal originates from the SRTM data set. A 2.7 m elevation change would translate to $\sim$1 mm in range change for a perpendicular baseline of 100 m. Therefore errors imposed on the interferograms from the USGS DEM are likely to be <1 mm.

[12] We minimize orbital gradients across the interferogram by utilizing coherent data from the entire SAR frame to flatten the phase. Orbital errors produce near-linear gradients across an interferogram. We use Precise Orbit Products provided by ESA as the initial parameters when calculating the orbital baseline. The regional gradient associated with the interseismic strain field across the bay area is removed using a dislocation model derived from available GPS data presented by *Bürgmann et al.* [2000]. Regions of isolated, coherent data located in the eastern regions of the bay area are connected by manually estimating the number of wavelength cycles represented by the deformation field across the incoherent gaps before an automated algorithm unwraps the phase. Orbital baseline values are then reestimated using the flattened interferogram and the interseismic gradient is added back to the interferogram. Each interferogram is geo-referenced to the USGS DEM and a subsection surrounding the Santa Clara valley is extracted for analysis. Finally, the range change is referenced to Oak Hill, an outcrop of consolidated bedrock located in the southern portion of the Santa Clara valley [*Wentworth et al.*, 1999],

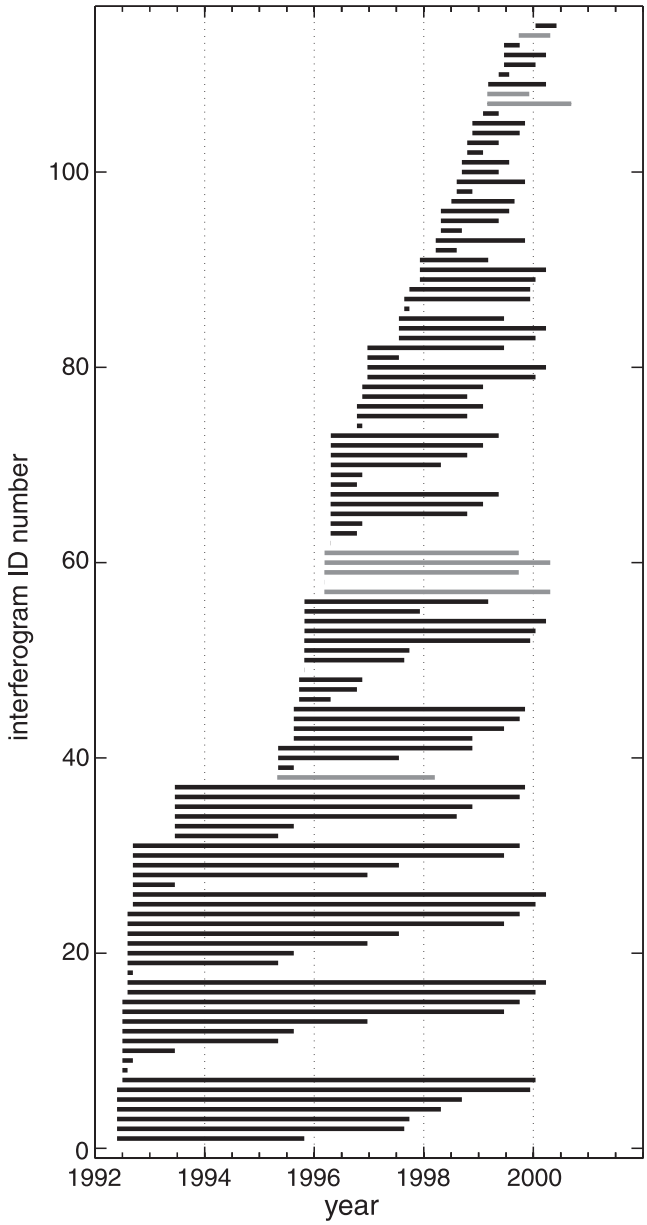

Figure 3. Temporal distribution of interferograms with perpendicular baselines of <200 m. These include all data acquired by the ERS-1/2 spacecraft from June 1992 to September 2000 along tracks 478 (gray horizontal bars) and 70 (black horizontal bars). A complete list of interferograms is given in the auxiliary material available online.[1]

which is assumed to be less susceptible to any groundwater-controlled deformation.

[13] A least squares inversion is performed that translates the set of interferograms into a range change time series that describes the time-dependent surface deformation. The linear inversion methodology is described in Appendix A. The time series is constructed by solving for the incremental range change between synthetic aperture radar (SAR) data acquisitions. The final time series has an irregular temporal sampling where each time step corresponds to the acquisition date of a SAR scene. The ERS spacecraft repeat their orbits every 35 days; however, longer gaps occur when acquisitions were not scheduled, orbit baselines were unsuitable, or the spacecraft orbital configuration was altered. A comparison of the time series result with individual interferograms illustrates the ability of the time series to fit the original data (Figure 4).

[14] The errors for the time series result are estimated by calculating the model variances [*Menke*, 1989]. We assume that the standard error for the range change observation is 0.004 m. Using the covariance of the least squares solution, the time series error σ_t at time t can be estimated using the generalized inverse $\mathbf{G}^{-g}$ (see Appendix A) and the identity matrix $\mathbf{I}$,

$$\Sigma = 0.004^2 \mathbf{G}^{-\mathbf{g}} \mathbf{I} (\mathbf{G}^{-\mathbf{g}})^{\mathbf{T}}, \tag{1}$$

$$\sigma_t = \sqrt{\sum_{k=1}^{t} \Sigma_{kk}}. \tag{2}$$

While this approach does not fully address the true covariance structure of the InSAR data, it does illustrate how errors are propagated through the inversion. Other data analysis techniques that derive estimates of the variance from the data, such as stacking, would produce smaller estimates of the standard error than those calculated above. However, for the time series inversion a higher error estimate is expected because the time-dependent signal is not constrained to a specific form. For example, stacking assumes that deformation rates are constant and this assumption acts as an additional constraint.

[15] The analysis of descending and ascending InSAR data, which use different look vectors, suggests that the observed deformation is predominantly vertical. Descending and ascending SAR data are collected by the ERS-1 and ERS-2 spacecraft along two different orbital tracks. Track 70 is on a descending trajectory with the satellite moving from north to south and the antenna looking to the northwest (look azimuth ~284°). Track 478 is on an ascending trajectory with the satellite moving from south to north looking to the northeast (look azimuth ~76°). The differing look vectors can be used to decipher vertical from horizontal deformation if one component of the three-dimensional deformation field can be independently constrained. Both the ascending and descending data are consistent with the assumption that the ground deformation is predominantly vertical. Since only 9 ascending interferograms are available, we were unable to quantitatively estimate any small component of horizontal deformation that might accompany uplift or subsidence. While the look angle varies across a SAR frame, we use the angle of 20° at the center of the valley and multiply the range change observations by 1.064 to project them onto a vertical unit vector.

4. Results for the Santa Clara Valley

[16] The InSAR time series reveals an overall pattern of uplift since 1992 with as much as 41 ± 18 mm of uplift centered north of Sunnyvale (Figure 5a). Most of this uplift occurs between 1992 and 1998 with a mean uplift rate of

[1] Supporting auxilliary material are available at ftp://agu.org/apend/jb/2002JB002267.

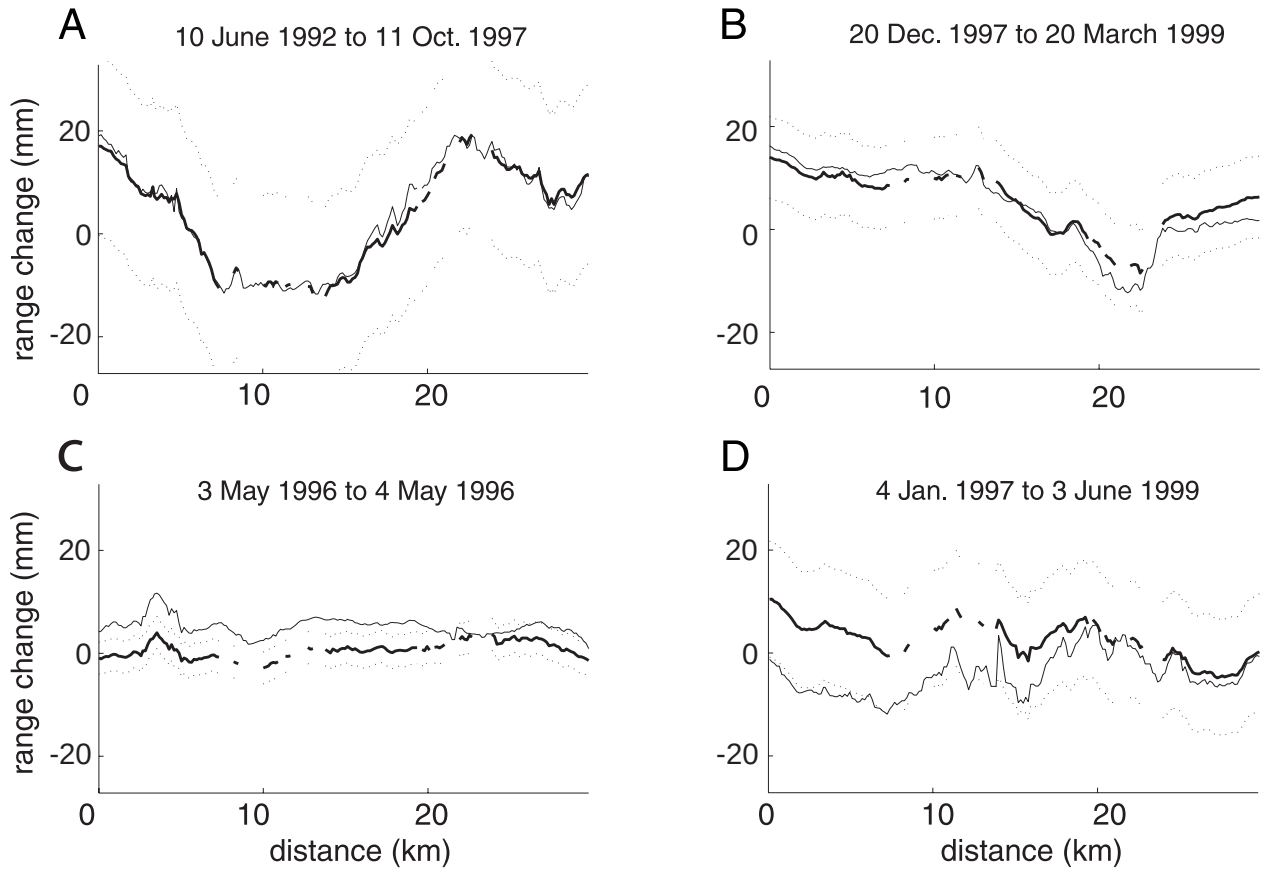

Figure 4. InSAR time series profiles (heavy solid line and dotted error envelope) compared to individual interferograms (thinner solid line) spanning the respective time interval. These plots provide a representative illustration of how closely the inversion reproduces the original InSAR data. Profiles correspond to the upper west-east level line path A-A′ in Figure 1. Most of the interferograms are fully reproduced as in Figures 4a and 4b. Several profiles show constant offsets or gradients between the interferograms and time series (Figures 4c and 4d) which are attributed to orbital or long-wavelength atmospheric artifacts.

6.4 ± 2.2 mm/yr. From Sunnyvale, the surface deformation extends along several major tributaries, especially along Calabazas and Saratoga creeks. An additional center of uplift is observed to the east of San Jose. The southwestern portion of the valley shows no distinctive pattern of deformation. Subsidence relative to Oak Hill is only observed along the western valley margin where the Plio-Pleistocene Santa Clara formation is found to outcrop.

[17] Accompanying the net uplift, a seasonal uplift pattern is resolved with the largest peak-to-trough fluctuations centered near San Jose (Figure 5b). The seasonal signal is sharply bounded to the east by a structure that aligns with the northward extension of the Silver Creek fault [*Ikehara et al.*, 1998]. Both ascending and descending interferograms show consistent deformation across this fault demonstrating that the relative motion is vertical and not related to strike-slip fault motion. The fault appears as a sharp discontinuity in the deformation field of several interferograms. A seasonal subsidence pattern is also observed in the northwest portion of the valley.

4.1. Evaluation of Spatial Accuracy

[18] The InSAR time series compares well with elevation changes measured using spirit leveling corroborating the inferred pattern of uplift. Level line data were collected in the valley beginning in 1912 [*Poland and Ireland*, 1988]. Since 1989 the Santa Clara Valley Water District has performed yearly leveling surveys across the valley (Figure 1). In 1999 a leveling route was added running west-to-east across the southern half of the valley and observations were increased to biyearly sampling. Cumulative deformation along each level line is compared to profiles across the InSAR time series (Figure 6). The shape of the profiles agrees well except for a significant discrepancy between kilometers 0 to 5 in Figure 6b. Differences between the InSAR time series and the level data may reflect additional subsidence during the time from when the level data were collected and when the SAR data were acquired, artifacts in the InSAR data, propagating errors along the leveling line, or the local motion of individual bench marks.

4.2. Evaluation of Temporal Accuracy

[19] The temporal evolution of the surface deformation agrees with the borehole extensometer data available at two locations. Extensometers which measure the sediment compaction and expansion were installed in the valley by the USGS in the early 1960s to study the relationship between head level, compaction, and subsidence [*Lofgren*, 1961].

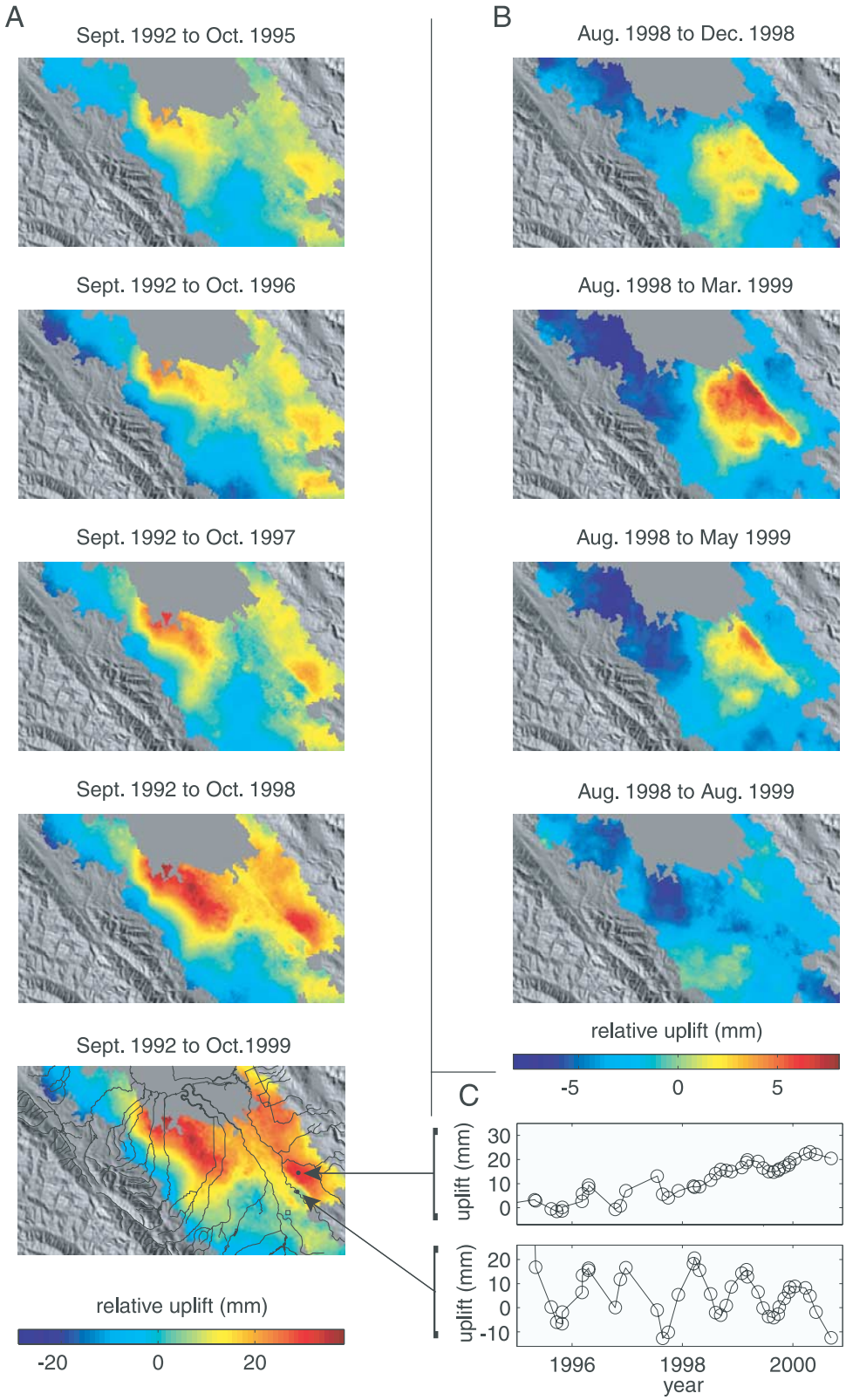

Figure 5. (a) Five frames from the InSAR time series show the pattern of cummulative uplift since September 1992 centered north of Sunnyvale and east of the Silver Creek fault near San Jose. Uplift is relative to Oak Hill (open square in final frame). The drainage network for the Santa Clara valley is also shown in the final frame. (b) Seasonal uplift pattern during a period from August 1998 to August 1999. (c) Comparison of time series at two points (dots in final frame of Figure 5a) illustrating the seasonal versus long-term deformation pattern partitioned by the Silver Creek.

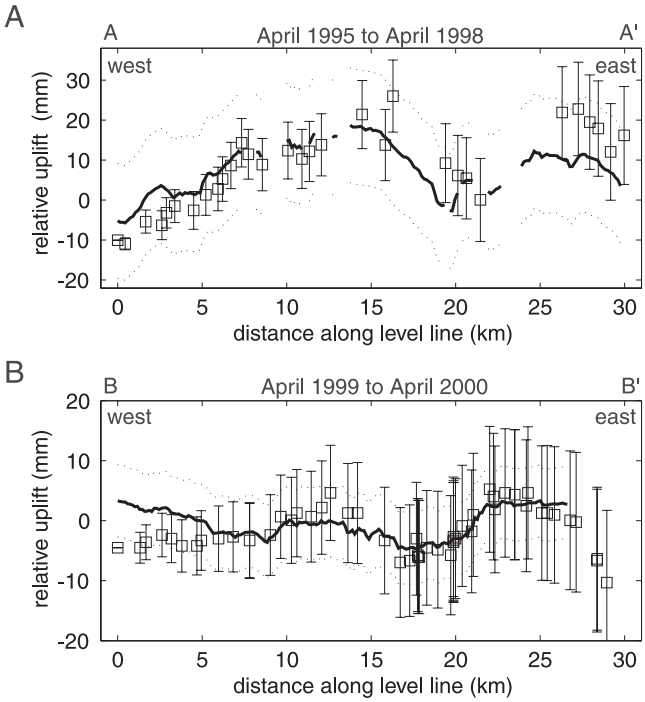

Figure 6. Comparison of leveling data (open squares with error bars) and the InSAR time series (solid line with dotted error envelope). (a) Elevation change from April 1995 to April 1998 along a west-to-east path from Los Altos to Milpitas (A-A′ in Figure 1). (b) Elevation change from April 1999 to April 2000 along a west-to-east path from Los Gatos to Alum Rock (B-B′ in Figure 1). Range change data are projected onto a vertical unit vector. Gaps in the InSAR profile reflect regions where the phase is incoherent and therefore no data are available. Since a common vertical reference does not exist for both data sets, the level line data are arbitrarily shifted vertically so that the profiles can be compared to the InSAR data. Errors in elevation change relative to the westernmost bench mark accumulate along the leveling line according to 2.24 mm/$\sqrt{km}$. The maximum change in topography (not shown) across the valley is 70 m, and most of this change is located near the edges of the valley.

The Santa Clara Valley Water District currently maintains extensometers at SUNNY and MARTHA which are anchored at a depth of 306 and 183 m, respectively (see Figure 1 for location). The temporal accuracy of the InSAR time series can be evaluated by comparing it to the compaction as measured by the extensometers. Both the trend and the magnitude of the seasonal oscillation agree between the two data sets (Figures 7a and 7b) and suggest that all seasonal deformation is confined within the depth range of the extensometer boreholes.

[20] Head levels which are sampled on a monthly basis at several wells are found to be highly correlated with the seasonal uplift. Head levels and compaction data can be used to calculate the elastic skeletal storage coefficient S_{ke} which describes the elastic response of the aquifer to a change in effective stress [*Lohman*, 1961]. The change in water level Δh is related to the change in compaction Δb according to $\Delta b = -\Delta h \times S_{ke}$. The uplift signal of the InSAR time series is compared to the compaction calculated for a well located near San Jose assuming $S_{ke} = 1.5 \times 10^{-3}$ as determined by *Poland and Ireland* [1988] (Figure 7c). The inferred compaction closely follows the measured uplift signal suggesting that the ongoing deformation is elastic.

5. Discussion

5.1. Interpretation of Uplift and Subsidence Pattern

[21] The Santa Clara Valley aquifer can be subdivided into several hydrogeologic units [*Carroll*, 1991; *Iwamura*, 1995]. The forebay region includes the alluvial fan deposits found along the perimeter of the valley where high vertical permeabilities allow surface water to infiltrate the aquifer. Groundwater then flows horizontally into the confined

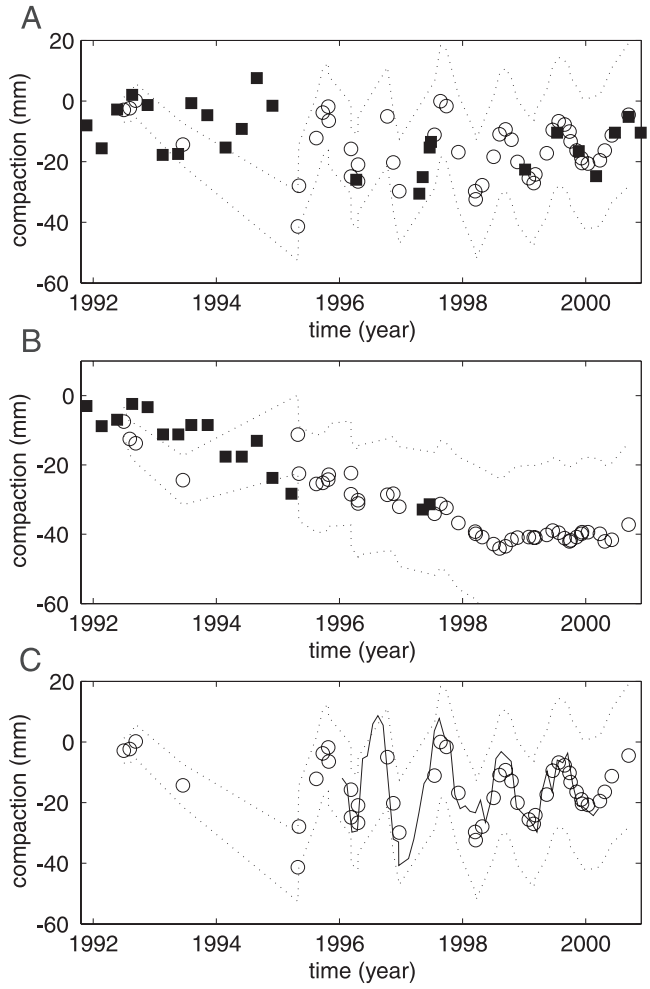

Figure 7. Comparison of extensometer observations (solid squares) and the InSAR time series (circles with dotted error envelope) for instruments (a) MARTHA and (b) SUNNY. (c) Comparison of the InSAR time series to well level depths that have been converted to compaction using the relationship discussed in the text for a well adjacent to the MARTHA extensometer (well 07S01E16C005, solid line). Well level data are collected approximately every month, providing a temporal sampling rate comparable to the InSAR time series.

zone, a region in the central part of the valley where water-bearing units are capped by thick layers of fine silt and clay which restrict the vertical flow of groundwater. The primary confined aquifer is located at a depth interval of 60–300 m and consists of unconsolidated alluvium over the semi-consolidated alluvium of the Plio-Pleistocene Santa Clara formation. Well log data and hydraulic head levels have identified a sequence of productive water-bearing units referred to as the Agnew aquifer [*California Department of Water Resources* (*CDWR*), 1967; *Johnson*, 1995], although several overlying aquifer and aquitards are found beneath the confined zone. The deposition of this structure is associated with the ancestral drainage of Coyote creek and the Guadalupe river, both of which transport sediment down the valley axis to the bay [*Meade*, 1967; *CDWR*, 1967]. The overall thickness of the aquifer is unconstrained for much of the valley because few of the wells reach the consolidated bedrock of the Franciscan complex. At several localities, such as in San Jose and north of Sunnyvale, the depth to basement is believed to be in excess of 420 m [*Meade*, 1967; *CDWR*, 1967]. Well data suggest that the depth to basement is highly variable throughout the San Francisco Bay region where faulting and erosion during periods of low sea level have created an irregular bedrock surface [*Atwater et al.*, 1977].

[22] The spatial pattern of land subsidence observed during the first half of the twentieth century correlates with the lateral extent of the confined aquifer. From 1934 to 1960, maximum subsidence was centered north of Sunnyvale and in the region directly east of San Jose (Figure 2) [*Poland and Ireland*, 1988; *Poland and Green*, 1962]. In the decade that followed, subsidence continued primarily in the vicinity of San Jose. The correlation of the land subsidence and the spatial extent of the confined aquifer is not surprising given that the greatest amount of compaction occurs in the fine-grade interbeds.

[23] The surface deformation observed from 1992 to 2000 reflects the poroelastic response of the confined aquifer resulting from the redistribution of groundwater. The long-term uplift and seasonal deformation revealed by the InSAR data are located within the limits of the confined aquifer. Analysis of head levels within different stratigraphic units suggest that pore pressure fluctuations within the confined aquifer can be considerably larger than that observed in the unconfined water table [*Carroll*, 1991]. This suggests that the confined aquifer is the predominant source of the deformation. As the seasonal recharge of groundwater begins to outpace withdrawal, head levels increase resulting in uplift.

[24] The surface deformation suggests that the aquifer can be further subdivided into different domains that are controlled by the distribution of hydrogeologic properties. Seasonal uplift and subsidence shown in Figure 5b outlines a region that broadens toward the north. The southern end of the seasonal uplift signal is colocated with the southernmost limit of the confined zone. Recharge of the basin is accommodated through the flow of subsurface water from the Coyote valley located to the south of the Santa Clara valley. Subsurface water flows through a narrow alluvial channel between Oak Hill and Edenvale Ridge from where it cascades into the deeper aquifer [*CDWR*, 1967]. Using statistical correlations between well perforation indicators, *Johnson* [1995] found that coarse-grained units are more abundant near San Jose than in Sunnyvale. Similarly, *Meade* [1967] and *Johnson et al.* [1968] found that fine sands and clays were more predominant in the stratigraphic column beneath Sunnyvale. This suggests that the two regions of the aquifer that exhibit different deformation styles also have different hydrogeologic properties. A higher permeability within and greater connectivity between permeable units beneath San Jose may facilitate the flow of groundwater to regions of the aquifer under lower confining pressures. The large seasonal uplift signal may reflect the rapid redistribution of groundwater whereas the long term uplift reflects the net increase in pore fluid pressure.

[25] While uplift is observed from 1992 to 2000, some interbeds may still experience compaction either as a consequence of the historical withdrawal of groundwater or from pumping during the summer months. Since the hydraulic conductivity of interbeds is low compared to the surrounding aquifer, the flow of groundwater out of the interbeds continues as long as hydraulic gradients persist. For example, in the 1960s, *Poland and Ireland* [1988] observed compaction to continue for up to a decade following the recovery of head levels. However, given that the surface deformation observed by the InSAR data is small (approximately centimeters), any compaction masked by the uplift signal from 1992 to 2000 is likely to be negligible.

5.2. Silver Creek Fault

[26] The differential subsidence across the Silver Creek fault suggests that the aquifer is partitioned at depth. Seasonal uplift and subsidence is observed on the west side of the fault while long term uplift occurs on the east side of the fault. The net uplift east of the Silver Creek fault may reflect the damming of groundwater from the eastern tributaries of the Santa Clara valley. The fault may bisect sections of the Agnew aquifer and prevent recharge from reaching the central portion of the aquifer. While faults can act as either low-permeability barriers that inhibit fluid flow or as conduits [e.g., *Caine et al.*, 1996], the Silver Creek fault clearly acts to partition the groundwater system. This can be accomplished either when lithologic units of different permeability are juxtaposed during faulting [*Maclay and Small*, 1983], when sedimentation varies across a syndepositionally active fault [*Aydin*, 2000], or by the grain size reduction and gouge development in the fault core [*Teufel*, 1987].

[27] The trace of the Silver Creek fault, which has been difficult to identify in the field, can be mapped using the InSAR data. The unconsolidated alluvium conceals much of the fault network present in the Franciscan bedrock below the Santa Clara valley. The identification of these faults provides important information that could ultimately be used to evaluate the seismic hazard for the region [*Rogers and Williams*, 1974]. The Silver Creek fault is of special concern because of its proximity to downtown San Jose. The fault was originally identified as a west dipping thrust fault separating geologic units of the Santa Clara formation and the Franciscan complex in exposed bedrock to the south. *Crittenden* [1951] postulated that the fault continued beneath the alluvium to the north, although evidence indicating whether the fault has exhibited movement since

the Holocene was inconclusive [*CDWR*, 1967; *Rogers and Williams*, 1974; *Bryant*, 1981; *Catchings et al.*, 2000]. The existence and location of the fault trace has been difficult to ascertain from hydrologic, geomorphic, or geophysical analyses. The fault trace is constrained within a 200-m-wide zone where the deformation resolved by InSAR is localized. A SAR amplitude image of the region with the fault trace mapped using the InSAR phase is included in the auxiliary material data set. The zone of deformation was chosen by manually looking for inflection or knick points in the range change. Deformation is evenly distributed within the zone, although discrete jumps in phase are observed at some locations.

[28] Although the hydraulically induced deformation pattern provides constraints on the fault's location, it is difficult to infer how much slip has been accommodated or when it was most recently active. The sharp lineament observed in the interferograms suggests that the fault penetrates the alluvium, which would suggest that the fault has been active since at least the deposition of the shallow aquifer. Using high-resolution gravity and magnetic data, *Jachens et al.* [2002] suggest that significant right-lateral slip has been accommodated along the Silver Creek fault as evidenced by the formation of an extensional basin to the east. Several km of offset along the Silver Creek fault may be sufficient to form a fault core capable of inhibiting fluid flow. However, offset lithologies observed by *Catchings et al.* [2000] from a seismic reflection survey could produce the same groundwater damming effect without significant shear along the fault.

6. Conclusions

[29] The recovery of groundwater levels which began in the 1960s appears to have continued through the 1990s as inferred from the regional uplift in the Santa Clara Valley. We observe 41 ± 18 mm of uplift centered north of Sunnyvale from 1992 to 2000. Uplift is also resolved east of San Jose where the Silver Creek fault has restricted the flow of groundwater to the west. While a small, latent subsidence signal may still persist, compaction does not appear to be a significant source of deformation.

[30] The temporal and spatial pattern of uplift and subsidence afforded by InSAR provides important constraints on the lateral distribution of water-bearing units and the time scales over which the groundwater is exchanged. A higher transmissivity allows for the rapid redistribution of groundwater beneath San Jose resulting in a large, seasonal deformation signal. Ultimately knowing the lateral extent and connectivity of water bearing units will improve numerical studies which attempt to model the mechanics of the aquifer system [e.g., *Wilson and Gorelick*, 1996; *Leake*, 1990; *CDWR*, 1967; *Helm*, 1977].

[31] We demonstrate how a complex, time-dependent signal can be extracted from a large InSAR data set. Our time series methodology does not parameterize the mode of deformation, whether it be linear, nonlinear, or sinusoidal, unlike previous time series approaches [i.e., *Ferretti et al.*, 2000]. The inversion also acts to reduce atmospheric and orbital artifacts inherent in each individual interferogram. It provides a tool that aids in the interpretation of complex deformation patterns with applications toward the study of tectonic, hydrologic, and volcanic systems.

Appendix A: InSAR Time Series

A1. Motivation

[32] Many earth deformation processes associated with faulting, volcanoes, and fluid withdrawal or injection exhibit nonlinear behavior. Transient relaxation processes following large earthquakes produce surface displacements that decay nonlinearly with time [*Bürgmann et al.*, 2002]. Deformation arising from volcanic inflation can be spatially and temporally variable and the observation of this complexity can provide valuable insight into the rate of fluid or magma movement within the subsurface [*Wicks et al.*, 1998]. Aseismic surface creep and slow earthquakes are additional examples of transient processes that are best resolved using data sets with high spatial and temporal resolution [*Lyons and Sandwell*, 2003].

[33] InSAR has the potential to resolve spatially and temporally complex deformation sources especially if redundant data can be used to separate the desirable deformation signal from noise and other artifacts, such as atmospheric delays [e.g., *Sandwell and Price*, 1998; *Zebker et al.*, 1997]. Many regions of study are also affected by more than one deformation process, such as land subsidence in combination with tectonic deformation [*Bawden et al.*, 2001; *Watson et al.*, 2002]. The existing catalogue of SAR data collected over the past decade provides an opportunity to observe complex, nonlinear deformation. We present a technique to extract a time-dependent deformation signal that synthesizes information contained in a large InSAR data set.

A2. Inversion Methodology

[34] We invert for a time series of range change by performing a least squares inversion of differential interferograms. The definitions of parameters for the following discussion are given in the notation section and are shown schematically in Figure A1. Vectors and matrices are denoted in bold where m_1 is the first element in vector **m** and G_{ij} corresponds to element (i, j) of matrix **G**. The incremental range change **m** between SAR acquisitions can be related to the InSAR data **d** according to

$$\mathbf{Gm} = \mathbf{d}. \tag{A1}$$

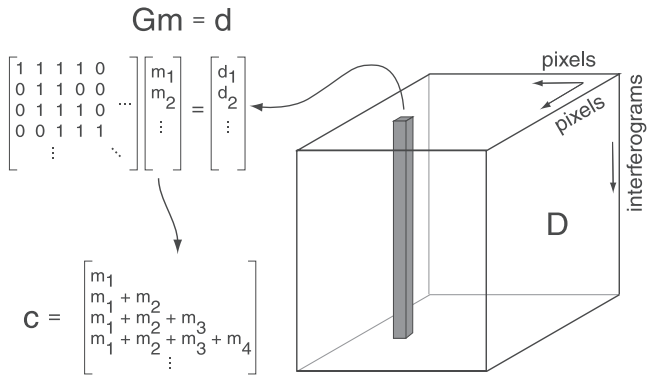

Figure A1. Schematic showing the relationship between data and model matrices in the inversion.

Using single value decomposition to find the generalized inverse of **G**, **m** can be solved directly [*Menke*, 1989]. The range change time series, **C**, is constructed by summing the incremental range change from preceding time steps,

$$C_t = \sum_{k=1}^{t} m_k. \tag{A2}$$

[35] The design matrix, **G**, is constructed from the temporal distribution of SAR scene acquisitions. Assume that the InSAR data set consists of N interferograms from S independent SAR scenes. The dates of the SAR scenes are contained in chronological order in the $1 \times S$ vector **L**. **H** is a $2 \times N$ matrix containing the beginning and ending date for each interferogram ordered by the date of the first scene. The incremental range change and the InSAR data are related through a combination of ones and zeros using the information in **H** and **L**,

$$G_{ij} = \begin{cases} 1 \text{ for } H_{i1} \le L_j < H_{i2} \\ 0 \text{ for } H_{i1} > L_j \text{or} L_j \ge H_{i2}. \end{cases} \tag{A3}$$

Interferograms must be colocated and of identical dimensions. The range change in each interferogram is referenced to a reference pixel to ensure that all deformation is measured relative to a common location. The range change data are contained in the three-dimensional matrix **D** where D_{ijk} is the (i, j) pixel of the kth interferogram. The data vector **d** contains the range change observation at a given pixel location (i, j), for all interferograms,

$$\mathbf{d} = \begin{bmatrix} D_{ij1} \\ \vdots \\ D_{ijN} \end{bmatrix}. \tag{A4}$$

The inversion discussed above is repeated at each pixel location where InSAR data are coherent for all interferograms.

[36] The acquisition rate of SAR scenes dictates the temporal resolution of the final time series, while the number and distribution of interferograms determines the model and data resolution of the inversion. Typically, the number of interferograms N is significantly greater than the number of SAR scenes S. As N approaches S, the inversion becomes less stable and it may become necessary to exclude those interferograms where a SAR scene is used only once. This helps to improve the model resolution matrix and stabilize the inversion at the expense of reducing the temporal resolution. We find that at least 30 interferograms are required to produce a reasonable time series.

[37] The utilization of redundant InSAR data, i.e., interferograms spanning similar time periods, helps to improve the model resolution of the inversion but also imposes a potential bias in the result. To avoid topography correlated errors into the interferograms, a maximum perpendicular baseline is typically chosen based on the quality of the DEM. This criteria limits the number of compatible SAR pairs making it difficult to find an independent set of interferograms. The calculation of the time series becomes a mixed-determined inverse problem where the inclusion of redundant data is crucial for improving the model resolution and assisting in the reduction of uncorrelated errors. However, SAR scenes that are more frequently utilized in the creation of interferograms have a greater impact in the inversion and could potentially bias the final time series. We investigated several schemes to weight the interferograms in an attempt to compensate for any bias imposed by individual SAR scenes. However, we found that weighting the interferograms based on scene usage did not significantly change the results of the inversion. We elected to treat each interferogram as independent data, acknowledging that interferograms that share common SAR scenes are partially correlated.

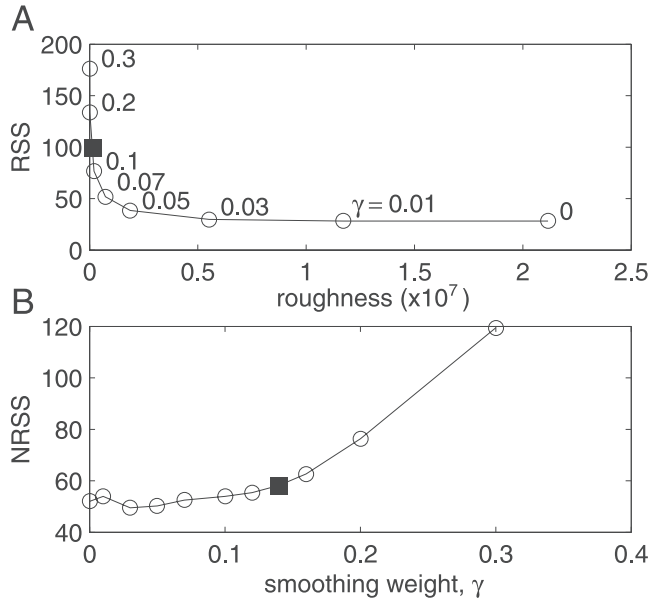

Figure A2. Determination of the smoothing parameter, γ, using (a) the trade-off between the residual sum of squares and the roughness and (b) the increase in the residual sum of squares between the compaction data (Figure 7c) and the time series as a function of γ. Ultimately, we use Figure A2b and the minimization of apparent atmospheric artifacts (Figure A3) to choose a value of $\gamma = 0.14$.

[38] SAR data collected by ERS include several inherent limitations when attempting to resolve time-dependent deformation. As with any time series, a regular and dense sampling rate is required to fully characterize a nonlinear signal. The irregular acquisition of ERS-1 and ERS-2 data remains a limitation when performing a time series analysis. For example, the InSAR time series of the seasonal uplift near San Jose does not fully capture the large peak-to-trough amplitude of the compaction signal in the early part of 1997 because of the gap in available data (Figure 7c). Complementary data sets, such as continuous GPS [*Bawden et al.*, 2001], can provide valuable information between SAR scene acquisitions when InSAR data are unavailable. Additionally, the ERS acquisitions largely consist of descending orbit data, limiting the potential for creating a separate time series of ascending SAR data to gain insight into the multidimensional displacement field.

A3. Reduction of Atmospheric Artifacts

[39] If the surface deformation is expected to be a smooth function of time, then a smoothing constraint can be used to

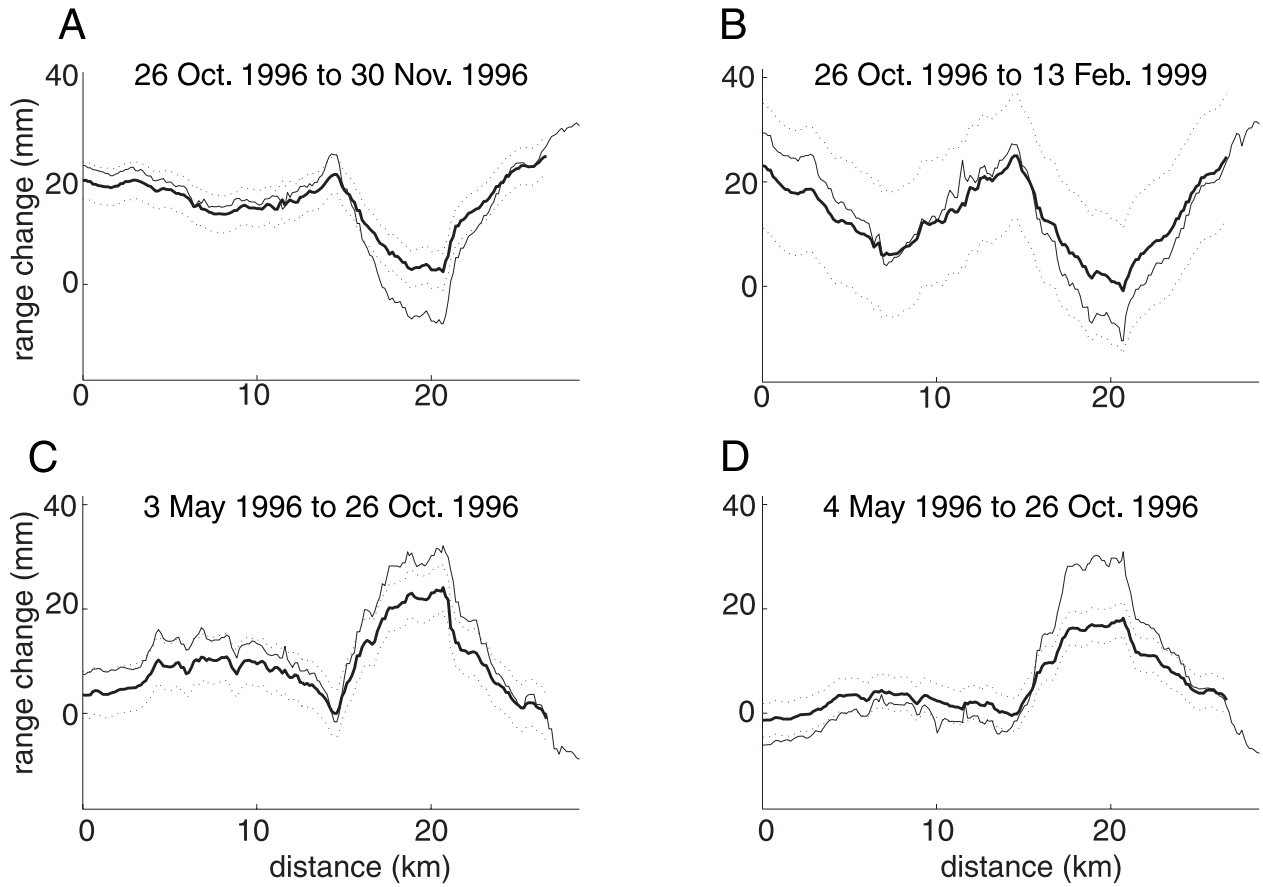

Figure A3. Comparison of the InSAR time series (heavy solid line with dotted error envelope) and range change observations from the original interferograms (thinner solid line). Profiles are taken along the lower west-east level line path B-B′ (Figure 1). An atmospheric artifact that creates a range change delay of ~10 mm is located at 20 km along the profile. The atmospheric delay occurs in the 16 October 1996 SAR acquisition and can be identified by examining those interferograms that use this SAR scene. Increasing the temporal smoothing parameter, γ, is found to reduce this artifact.

minimize atmospheric artifacts. Interferograms are often plagued by atmospheric artifacts which constitute the greatest source of error with InSAR [*Zebker et al.*, 1997; *Hanssen*, 2001]. Any phase delay resulting from the lateral heterogeneity of the index of refraction in the atmosphere would ideally be estimated and removed from the interferograms using a priori zenith delays determined from meteorological data or continuous GPS [*Williams et al.*, 1998]. Unfortunately, this information is not readily available at the required spatial or temporal resolution to be feasible for this study. In the time series analysis atmospheric artifacts produce discrete jumps that can be eliminated by assuming that range change accelerations between time steps are small.

[40] Temporal smoothing is enforced using a finite difference approximation. The smoothing constraint assumes less deformation to occur during short time periods, as would be expected for short duration interferograms (i.e., tandem pair interferograms). Thus by including a smoothing constraint, atmospheric artifacts will be minimized depending on how strongly temporal smoothing is enforced. The smoothing constraint is incorporated into the inversion by augmenting the linear equation relating the InSAR data $\mathbf{d}$ and the incremental range change $\mathbf{m}$,

$$\begin{bmatrix} \mathbf{G} \\ \gamma^2 \frac{d}{dt} \end{bmatrix} \mathbf{m} = \begin{bmatrix} \mathbf{d} \\ 0 \end{bmatrix}. \tag{A5}$$

The degree of smoothing is determined by the factor γ, where $\gamma = 0$ corresponds to no smoothing. A direct inversion of the interferograms without imposing the smoothing constraint produces a time series that is rough and prone to sharp fluctuations from one time step to the next while a γ that is too large will dampen the deformation signal.

[41] The choice of the smoothing weight is largely subjective but can be evaluated using external data sets. We attempted to use a cross-validation sum of squares (CVSS) as demonstrated by *Matthews and Segall* [1993] for determining the proper weight applied to the smoothing operator. The CVSS did not produce a minimum and therefore, did not constrain γ. We chose a γ equal to 0.14 such that the residual sum of squares (RSS = $|\mathbf{d} - \mathbf{Gm}|_2$) is minimized while also minimizing any atmospheric artifacts that were identified through direct inspection of the interferograms (Figure A2). Auxiliary data sets, such as extensometer, leveling, or GPS data, help to evaluate whether the model is oversmoothed. A significant fraction of the roughness can be attributed to atmospheric artifacts that can produce a range change greater than 10 mm.

[42] To assess whether the time series inversion is successful at minimizing atmospheric artifacts, we examine a set of interferograms that share a common SAR scene (Figure A3). The apparent elevation change for an atmospheric artifact is spatially correlated with a similar magnitude range change for all interferograms that utilize the common scene. The sign of the artifact flips depending on whether the scene is the first or second scene in the interferogram. While we can not rule out that a signal associated with a single scene is in fact due to a sudden and completely reversed deformation event, temporal smoothing acts to reduce such excursions.

Notation

- u, v number of pixels along the width and length of an interferogram.
- S number of SAR scenes.
- N number of interferograms in data set.
- $\mathbf{D}$ ($u \times v \times$ N) matrix containing the range change data.
- $\mathbf{L}$ ($S \times 1$) vector with the dates of the SAR scenes.
- $\mathbf{H}$ ($N \times 2$) array with the date of the first and second pass for each interferogram.
- $\mathbf{d}$ ($S \times 1$) range change date from all interferograms at a common pixel.
- $\mathbf{G}$ ($N + S - 2 \times S$) design matrix.
- γ smoothing factor.
- $\mathbf{m}$ ($S \times 1$) incremental range change between SAR acquisitions for a given pixel location.
- $\mathbf{C}$ ($S \times 1$) cumulative time series for a given pixel location.
- σ ($S \times 1$) vector with the propagated time series error.

[43] **Acknowledgments.** We would like to thank Mark Merritt of the Santa Clara Valley Water District for providing level line, extensometer, and well level data sets. This manuscript benefited from early comments by Devin Galloway. Reviews by David Sandwell, Gerald Bawden, and an anonymous reviewer helped to improve the organization and focus. SAR data were provided to the WInSAR Consortium by the European Space Agency (ESA) through their North American distributor, Eurimage. Original SAR data are copyrighted by ESA (1992–2000). Additional data provided by an ESA (ENVISAT) data grant. Funding for this work was provided by NASA grant NAG5-7580, and USGS NEHRP grant 02HQGR0062. Berkeley Seismological Laboratory contribution 03–04.

References

Alley, W., R. Healy, J. W. LaBaugh, and T. E. Reilly, Flow and storage in ground water systems, *Science*, *296*, 1985–1990, 2002.

Amelung, F., D. L. Galloway, J. W. Bell, H. A. Zebker, and R. J. Laczniak, Sensing the ups and downs of Las Vegas-InSAR reveals structural control of land subsidence and aquifer-system deformation, *Geology*, *27*, 483–486, 1999.

Atwater, B. F., C. W. Hedel, and E. J. Helley, Late Quarternary depositional history, Holocene sea-level changes, and vertical crustal movement, southern San Francisco Bay, California, *U.S. Geol. Surv. Prof. Pap.*, *1014*, 1–15, 1977.

Aydin, A., Fractures, faults, and hydrocarbon entrapment, migration, and flow, *Mar. Pet. Geol.*, *17*, 797–814, 2000.

Bawden, G. W., W. Thatcher, R. S. Stein, K. W. Hudnut, and G. Peltzer, Tectonic contraction across Los Angeles after removal of ground water pumping effects, *Nature*, *412*, 812–815, 2001.

Beauducel, F., P. Briole, and J. Froger, Volcano-wide fringes in ERS synthetic aperture radar interferograms of Etna (1992–1998): Deformation or tropospheric effect?, *J.Geophys. Res.*, *105*, 16,391–16,402, 2000.

Bryant, W. A., Southeast segment of Hayward, Evergreen, Quimby, Silver Creek, and Piercy fault, *Fault Eval. Rep. FER-106*, 20 pp., Calif. Div. of Mines and Geol., Sacramento, 1981.

Bürgmann, R., D. Schmidt, R. M. Nadeau, M. d'Alessio, E. Fielding, D. Manaker, T. V. McEvilly, and M. H. Murray, Earthquake potential along the northern Hayward fault, California, *Science*, *289*, 1178–1182, 2000.

Bürgmann, R., S. Ergintav, P. Segall, E. H. Hearn, S. McClusky, R. E. Reilinger, H. Woith, and J. Zschau, Time-dependent distributed afterslip on and deep below the Izmit earthquake rupture, *Bull. Sesol. Soc. Am.*, *92*, 126–137, 2002.

Caine, J. S., J. P. Evans, and C. B. Foster, Fault zone architecture and permeability structure, *Geology*, *24*, 1025–1028, 1996.

California Department of Water Resources (CDWR), Evaluation of ground water resources, South San Francisco Bay, appendix A: Geology, *Bull. 118-1*, 153 pp., Sacramento, 1967.

California Department of Water Resources (CDWR), Reconnaissance investigation of ground water storage in Santa Clara valley to increase yield of the State Water Project, report, 308 pp., Sacramento, 1985.

Carroll, G. R., Hydrogeologic analysis of the Santa Clara Valley groundwater basin, M.S., thesis, 267 pp., Stanford Univ., Stanford, Calif., 1991.

Catchings, R. D., M. R. Goldman, G. Gandhok, M. J. Rymer, and D. H. Underwood, Seismic imaging evidence for faulting across the northwestern projection of the Silver Creek fault, San Jose, California, *U.S. Geol. Surv. Open File Rep., 00-125*, 29 pp., 2000.

Clark, W. O., Ground water in Santa Clara valley, California, *U.S. Geol. Surv. Water Supply Pap.*, *519*, 209 pp., 1924.

Crittenden, M. D., Geology of the San Jose-Mount Hamilton area, California, *Bull. Calif. Div.*, 157, 1951.

Ferretti, A., C. Prati, and F. Rocca, Nonlinear subsidence rate estimation using permanent scatters in differential SAR interferometry, *IEEE Trans. Geosci. Remote Sens.*, *39*(5), 2202–2212, 2000.

Fielding, E. J., R. G. Blom, and R. M. Goldstein, Rapid subsidence over oil fields measured by SAR interferometry, *Geophys. Res. Lett.*, *25*, 3215–3218, 1998.

Fowler, L. C., Economic consequences of land surface subsidence, *J. Irrigat. Drain. Div. Am. Soc. Civ. Eng.*, *107*(IR2), 151–158, 1981.

Gabriel, A. K., R. M. Goldstein, and H. A. Zebker, Mapping small elevation changes over large areas-differential radar interferometry, *J. Geophys. Res.*, *94*, 9183–9191, 1989.

Galloway, D. L., K. W. Hudnut, S. E. Ingebritsen, S. P. Phillips, G. Peltzer, F. Rogez, and P. A. Rosen, Detection of aquifer system compaction and land subsidence using interferometric synthetic aperture radar, Antelope valley, Mojave Desert, California, *Water Resour. Res.*, *34*, 2573–2585, 1998.

Goldstein, R. M., and C. L. Werner, Radar interferogram filtering for geophysical applications, *Geophys. Res. Lett.*, *25*, 4035–4038, 1998.

Hanssen, R. F., *Radar Interferometry: Data Interpretation and Error Analysis*, 308 pp., Kluwer Acad., Norwell, Mass., 2001.

Helm, D. C., Estimating parameters of compacting fine-grained interbeds within a confined aquifer system by a one-dimensional simulation of field observations, in *Land Subsidence: Proceedings of the Second International Symposium on Land Subsidence held at Anaheim, December 1976, IAHS Publ., 121*, 145–156, 1977.

Hoffmann, J., H. Zebker, D. Galloway, and F. Amelung, Seasonal subsidence and rebound in Las Vegas valley, Nevada, observed by synthetic aperture radar interferometry, *Water Resour. Res.*, *37*, 1551–1566, 2001.

Ikehara, M. E., D. L. Galloway, E. Fielding, R. Bürgmann, A. S. Lewis, and B. Ahmadi, InSAR imagery reveals seasonal and longer-term land-surface elevation changes influenced by ground-water levels and fault alignment in Santa Clara valley, California, *Eos. Trans. AGU*, *79*(45), Fall Meet. Suppl., F37, 1998.

Iwamura, T. I., Hydrogeology of the Santa Clara and Coyote valleys ground water basins, California, in *Recent Geologic Studies in the San Francisco Bay Area*, edited by E. S. Sangines, D. A. Anderson, and A. V. Busing, *Publ. 76*, pp. 173–192, Pac. Sect., Soc. of Econ. Paleontol. and Mineral., Santa Barbara, Calif., 1995.

Jachens, R. C., C. M. Wentworth, R. M. Graymer, R. J. McLaughlin, and F. C. Chuang, A 40-km-long concealed basin suggests large offset on the Silver Creek fault, Santa Clara valley, California, *Geol. Soc. Am. Abstr. Programs*, *34*(5), 99, 2002.

Jennings, C. W., Fault activity map of California and adjacent areas: with locations and ages of recent volcanic eruptions, *Map 6*, scale 1:750,000, Calif. Div. of Mines and Geol., Sacramento, 1994.

Johnson, A. I., R. P. Moston, and D. A. Morris, Physical and hydrologic properties of water-bearing deposits in subsiding area in central California, *U.S. Geol. Surv. Prof. Pap.*, *497-A*, 71 pp., 1968.

Johnson, N. M., Deterministic and stochastic approaches for evaluating multiple scales of Santa Clara valley hydrostratigraphy, in *Recent Geologic Studies in the San Francisco Bay Area*, edited by E. S. Sangines, D. A. Anderson, and A. V. Busing, Publ. 76, pp. 193–208, Pac. Sect., Soc. of Econ, Paleontol. and Mineral., Santa Barbara, 1995.

Lanari, R., G. De Natale, P. Berardino, E. Sansosti, G. P. Ricciardi, S. Borgstrom, P. Capuano, F. Pingue, and C. Troise, Evidence for a peculiar style of ground deformation inferred at Vesuvius volcano, *Geophys. Res. Lett.*, *29*(9), 1292, doi:10.1029/2001GL014571, 2002.

Leake, S. A., Interbed storage changes and compaction in models of regional ground water flow, *Water Resour. Res.*, *26*, 1939–1950, 1990.

Lofgren, B. E., Measurement of compaction of aquifer systems in areas of land subsidence, *U.S. Geol. Surv. Prof. Pap.*, *424-B*, 49–52, 1961.

Lohman, S. W., Compression of elastic artesian aquifers, *U.S. Geol. Surv. Prof. Pap.*, *424-B*, 47–49, 1961.

Lyons, S., and D. Sandwell, Fault creep along the southern San Andreas from interferometric synthetic aperture radar, permanent scatters, and stacking, *J. Geophys. Res.*, *108*(B1), 2047, doi:10.1029/2002JB001831, 2003.

Maclay, R. W., and T. A. Small, Hydrostratigraphic subdivisions and fault barriers of the Edwards Aquifer, south-central Texas, *J. Hydrol.*, *61*, 127–146, 1983.

Massonnet, D., M. Rossi, C. Carmona, F. Adragna, G. Peltzer, K. Feigl, and T. Rabaute, The displacement field of the Landers earthquake mapped by radar interferometry, *Nature*, *364*, 138–142, 1993.

Massonnet, D., T. Holzer, and H. Vadon, Land subsidence caused by the East Mesa Geothermal Field, California, observed using SAR interferometry, *Geophys. Res. Lett.*, *24*, 901–904, 1997.

Matthews, M. V., and P. Segall, Statistical inversion of crustal deformation data and estimation of the depth distribution of slip in the 1906 earthquake, *J. Geophys. Res.*, *98*, 12,153–12,163, 1993.

Meade, R. H., Petrology of sediments underlying areas of land subsidence in central California, *U.S. Geol. Surv. Prof. Pap., 497-C*, 83 pp., 1967.

Menke, W., *Geophysical Data Analysis: Discrete Inverse Theory*, 289 pp., Academic, San Diego, Calif., 1989.

Poland, J. F., and G. H. Davis, Land subsidence due to withdrawal of fluids, *Rev. Eng. Geol.*, *2*, 187–269, 1969.

Poland, J. F., and J. H. Green, Subsidence in the Santa Clara valley, California, a progress report, *U.S. Geol. Surv. Water-Supply Pap.*, *1619-C*, 16 pp., 1962.

Poland, J. F., and R. L. Ireland, Land subsidence in the Santa Clara valley, California, as of 1982, mechanics of aquifer systems, *U.S. Geol. Surv. Prof. Pap.*, *497-F*, 61 pp., 1988.

Rice, J. R., and M. P. Cleary, Some basic stress diffusion solutions for fluid saturated elastic porous media with compressible constituents, *Rev. Geophys.*, *14*, 227–241, 1976.

Rogers, T. H., and J. W. Williams, Potential seismic hazards in Santa Clara County, California, *Spec. Rep. Calif. Div Mines Geol.*, *107*, 39 pp., 6 plates, 1974.

Sandwell, D. T., and E. Price, Phase gradient approach to stacking interferograms, *J. Geophys. Res.*, *103*, 30,183–30,204, 1998.

Teufel, L. W., Permeability changes during shear deformation of fractured rock, *Proc. U.S. Rock Mech. Symp.*, *28th*, 473–480, 1987.

Watson, K. M., Y. Bock, and D. T. Sandwell, Satellite interferometric observations of displacements associated with seasonal groundwater in the Los Angeles basin, *J. Geophys. Res.*, *107*(B4), 2074, doi:10.1029/2001JB000470, 2002.

Wentworth, C. M., M. C. Blake Jr., R. J. McLaughlin, and R. W. Graymer, Preliminary geologic description of the San Jose 30 × 60 minute quadrangle, California, *U.S. Geol. Surv. Open File Rep.*, *98-795,* 1999.

Wicks, C., W. Thatcher, and D. Dzurisin, Migration of fluids beneath Yellowstone caldera inferred from satellite radar interferometry, *Science*, *282*, 458–462, 1998.

Williams, S., Y. Bock, and P. Fang, Integrated satellite interferometry: Tropospheric noise, GPS estimates and implications for interferometric synthetic aperture radar products, *J. Geophys. Res.*, *103*, 27,051–27,067, 1998.

Wilson, A. M., and S. Gorelick, The effects of pulsed pumping on land subsidence in the Santa Clara valley, California, *J. Hydrol.*, *174*, 375–396, 1996.

Zebker, H. A., P. A. Rosen, and S. Hensley, Atmospheric effects in interferometric synthetic aperture radar surface deformation and topographic maps, *J. Geophys. Res.*, *102*, 7547–7563, 1997.

R. Bürgmann, Department of Earth and Planetary Science, University of California Berkeley, 307 McCone Hall, Berkeley, CA 94720-4767, USA. (burgmann@seismo.berkeley.edu)

D. A. Schmidt, Department of Geological Sciences, 1272 University of Oregon, Eugene, OR 97403-1272, USA. (das@uoregon.edu)